Journal of Materials Processing Technology 215 (2015) 299–308

Contents lists available at ScienceDirect

Journal of Materials Processing Technology

journal homepage: www.elsevier.com/locate/jmatprotec

Bonding strength of multiple SiC die attachment prepared by sintering of Ag nanoparticles

Jianfeng Li[a,*], Christopher Mark Johnson[a], Cyril Buttay[b], Wissam Sabbah[c], Stéphane Azzopardi[c]

[a] Department of Electrical and Electronic Engineering, The University of Nottingham, University Park, Nottingham NG7 2RD, United Kingdom
[b] Université de Lyon, CNRS, UMR5005, INSA-Lyon, Laboratoire Ampère, F-69621, France
[c] IMS Laboratory, Bordeaux Institute of Technology, 351 Cours de la Libération, F-33405 Talence, France

ARTICLE INFO

Article history:
Received 24 May 2014
Received in revised form 29 July 2014
Accepted 1 August 2014
Available online 11 August 2014

Keywords:
Nanoscale silver paste
Sintering
Shear strength
SiC power die attachment

ABSTRACT

3 mm × 3 mm dummy SiC dies with 100\200\200 nm thick Ti\W\Au metallization have simultaneously been attached using sintering of Ag nanoparticle paste on AlN-based direct bonded copper substrates with 5\0.1 μm thick NiP\Au finish. The effect of preparation and sintering parameters including time of drying the printed paste, sintering temperature and time, and pressure, on the average shear strength for multiple die attachments was investigated. The surfaces of the die attachments after the shear tests were observed and the individual shear strength values correlated with the "apparent" porosity and thicknesses of the corresponding die attachments (sintered layer). The results obtained are further discussed and compared with typical data reported in existing literature. Main conclusions include: (i) the present shear strength values and their variations are comparable with those reported for single die attachment samples, (ii) the effects of sintering parameters can be ascribed to the effectiveness of the organic content burnout and appropriate rate of growth and coalescence of the Ag nanoparticles during the sintering process, and (iii) thickness values of the sintered Ag die attachments may be taken as non-destructive measurements to monitor/evaluate the quality of die attachment during power electronic module manufacturing/assembly process.

1. Introduction

Wide band-gap semiconductor devices such as SiC power devices provide great opportunities to develop power electronic systems with increased power densities, high reliability in extreme environments and higher integration. For example, Kaminski (2012) reviewed the performance of commercially available SiC and GaN power devices, and confirmed their advantages for high switching speed and high-temperature operations. Hamada (2012) presented the development of SiC device and power module technologies for applications in environmentally friendly vehicles, and reported the power density of the intelligent power module in the Toyota's recent hybrid vehicles being increased year by year. However, the eutectic or near eutectic Sn–Ag and Sn–Ag–Cu solders that are more commonly used for power die attachments are not reliable for high power density and high-temperature power electronic applications. Mannan and Clode (2004) indicated that Sn–Ag–Cu solder joints are not suitable for long-term usage at elevated temperature due to crack formation at the intermetallic (IMC)-solder interface. This is in agreement with the fact that the eutectic, or near eutectic, Sn–Ag and Sn–Ag–Cu solders are prone to creep at elevated temperatures and the accumulation of plastic strain leads to crack initiation and propagation. Laurila et al. (2005) pointed out that a thick IMC layer at the solder/conductor metal interface may degrade the reliability of the solder joints, due to their inherent brittle nature and the tendency to generate structural defects. Therefore, rapid growth of IMCs between the solders and the metallization on both the devices and the substrates for high-temperature applications may also result in brittle fracture of the joints.

To address the increasing challenge of reliability problems for solder alloys and conductive adhesives commonly used for semiconductor die attachments in high-temperature and high reliability applications, several alternatives have been proposed. Li et al. (2012) summarized these alternatives in a previous paper, including transient liquid phase (TLP) soldering, sintering of Ag particles and nanoparticles, nanoparticle reinforced solders, emerging solder alloys, local brazing and liquid solder joint. They have

* Corresponding author. Tel.: +44 115 846 6890; fax: +44 115 951 5616.
E-mail addresses: Jianfeng.Li@nottingham.ac.uk, ljfwxy@yahoo.com (J. Li).

http://dx.doi.org/10.1016/j.jmatprotec.2014.08.002

been under intensive investigation and have demonstrated their potential, as evident from the following examples. Lugscheider and Ferrara (2004) achieved low-temperature Cu–SnIn, Cu–SnBi and Cu–InBi TLP joints with mechanical strength up to 40 MPa. The effect of soldering time on joining zone morphology and mechanical strength was also experimentally revealed. Ide et al. (2005) proposed a novel bonding process using Ag metallo-organic nanoparticles, and achieved Cu-to-Cu joints with shear strengths of 25–40 MPa, at a low sintering temperature of 300 °C and a sintering pressure of 1 or 5 MPa. Amagai (2008) evaluated a number of metallic nanoparticles as additions into Sn–Ag based solder alloys and found that Co, Ni and Pt nanoparticles were very effective for reducing the growth of IMC in the solder joints after the solder reflow process and during thermal ageing. Takaku et al. (2009) reported the high reliability of the emerging Zn–Al(–Cu) solder alloys for high-temperature applications. This could be attributed to the extremely slow increase in the thickness of the Al_3Ni_2 IMC layer formed between the Zn–Al(–Cu) solder alloys and the Ni substrate during soldering, ageing, and thermal cycling. Wang et al. (2003) described a local brazing process with nanostructured Al/Ni multilayer foils, and accomplished room-temperature soldering of stainless steel specimens with a shear strength of 48 MPa. Li et al. (2007) investigated the dissolution and interfacial reaction of Nb in contact with the liquid 52In–48Sn solder for high-temperature applications. A model based on diffusion-controlled nucleation and growth of $NbSn_2$ IMCs was established to explain the observed extremely slow kinetics of dissolution and interfacial reaction.

Of the above-mentioned alternative joining materials and technologies, sintering of Ag nanoparticles has so far received the most attention. Unlike traditional solder reflow processes, where solder joints are formed through liquid wetting, solid–liquid interfacial reaction and solidification, sintering is a process where bonding is achieved through atomic diffusion and particle consolidation. Therefore, due to the high melting point of pure Ag (about 960 °C), the sintered Ag joints can be produced at relatively low temperatures (below 300 °C), but used at elevated temperatures. Schwarzbauer (1987) invented the sintering of micron-sized Ag particles used for mounting electronic devices. To achieve dense, higher conductive and highly reliable sintered Ag joints at temperatures below 300 °C, a quasi-hydrostatic pressure of 30–50 MPa was generally applied to shorten the sintering process down to a few minutes. Zhang and Lu (2002) made a significant advance in this joining technology by replacing the micron-sized Ag particles with Ag nanoparticles. Ide et al. (2005) investigated the mechanism of metal-metal bonding process using Ag metallo-organic nanoparticles. Bai and Lu (2006) and Bai et al. (2007) obtained high quality sintered Ag joints at temperatures below 275 °C and under pressures of only a few MPa where even pressure-less sintering was achieved. They also demonstrated high reliability in small power die attachment, e.g., 1.7 mm × 1.4 mm and 3 mm × 3 mm SiC power die, for high-temperature applications.

Since then, research into the sintering of Ag nanoparticles for applications in power die attachment has been prolific, and here several representative examples are given from a wealth of studies reported in the existing literature. Akada et al. (2008) used the same formulation of the Ag metallo-organic nanoparticle paste to compare the interfacial bonding mechanisms to bare Cu and Cu plated with 2\0.7 μm thick Ni\Au. Their results indicated that epitaxial layer of Ag was only observed at the Ag\Au interface though good metallurgical joints could be formed on both Cu and Au surfaces. Buttay et al. (2011) considered the effects of surface roughness and metallization of substrate on the shear strength of sintered Ag joints, and noticed that the high surface roughness of some commercially available ceramic-based substrates might lead to the formation of large voids in the sintered Ag layers and hence low shear strength of the sintered Ag joints. Zheng et al. (2012) employed a double print process of printing Ag paste for large die attachment (e.g. >100 mm^2), and obtained an average shear strength of the sintered Ag joints in excess of 40 MPa. Wereszczak et al. (2012) compared the effect of surface topology of substrate and pattern of the printed Ag paste on the quality of the sintered Ag joints, and concluded that both the topological modification to the substrate and the use of a proper pattern of the printed Ag paste could increase the shear strength. Le Henaff et al. (2012) tested the thermal cycling reliability of the sintered Ag joints for attaching both Si and SiC dies, and found no appreciable degradation in the thermal resistance, impedance and cross-sections analyses after 2400 thermal cycles between −40 °C and 125 °C. Kraft et al. (2012) tested the power cycling reliability of Si diode samples with top and bottom side Ag sintering on direct bonded copper (DBC) substrates, revealing a lifetime 17 times longer than the soldered and wire bonded DBC samples. Li et al. (2013) investigated the mechanical and thermo-mechanical properties of the Ag nanoparticle paste sintered lap shear joint by cyclic shear test, and the results obtained can be used to explain and simulate the mechanical and thermo-mechanical response and the time-dependent inelastic strain development within the sintered Ag joints for power die attachment in certain application environments.

The quality of the sintered Ag joints depends on the formulation of the paste, consisting of Ag particles or nanoparticles, organic dispersant, binder and thinner, and the sintering parameters such as heating rate, sintering temperature, pressure and time. In the aforementioned literature, shear strengths of sintered Ag joints were commonly used as indicators for rapid selection and/or optimization of the sintering parameters, and in most cases the tests were carried out on single chip attachment samples. This is easily understood because the pressure applied on a single chip can be more accurately controlled than that applied on multiple die. However, in realistic applications, a number of die is often attached on one substrate simultaneously. Therefore, it is important to understand the dependence of the shear strength on sintering parameters for multiple die attachments.

In the present work, the shear strengths of multiple SiC die attachments on AlN direct bonded copper (DBC) substrates using sintered Ag nanoparticles have been investigated. The experimental sintering parameters have been arranged according to a statistical design. The objectives of this paper are therefore: (1) to explore the effects of sintering parameters on the average shear strength; (ii) to compare the average values and variations of the shear strength results with those reported in existing literature; (iii) to correlate the individual shear strength values with a type of "apparent" porosity and thickness values of the corresponding sintered Ag joints; and (iv) to propose a qualitative measurement of the thickness of the sintered Ag joint, which may be used for non-destructive monitoring of the quality of die attachment during the manufacturing/assembly process.

2. Materials and methods

2.1. Materials and components

Samples having 6 or 4 SiC dies attached on one AlN direct bonded copper (DBC) substrate using Ag sintering were prepared for the shear tests. The Ag nanoparticle paste used in the present work was obtained from Cookson Electronics (South Plainfield, NJ 07080, USA). This paste has been formulated for pressure-assisted die attachment on Ag or Au finish, and can be applied to attach both large and small die. In the present work, small 3 mm × 3 mm × 0.35 mm dummy SiC dies were used for shear tests.

The dummy SiC dies were obtained from one 3-inch SiC wafer with 100\200\200 nm thick Ti\W\Au sputtered on one side as

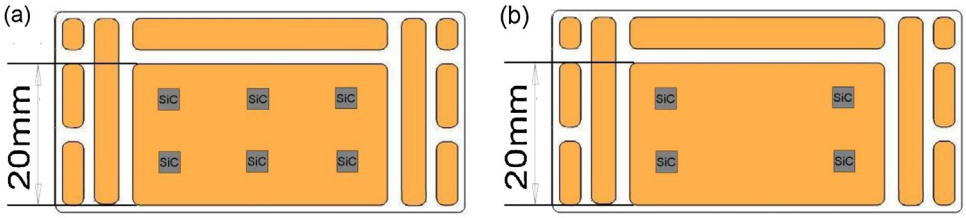

Fig. 1. Layouts of (a) 6 and (b) 4 of 3 mm × 3 mm dummy SiC dice on one AlN-based DBC substrate.

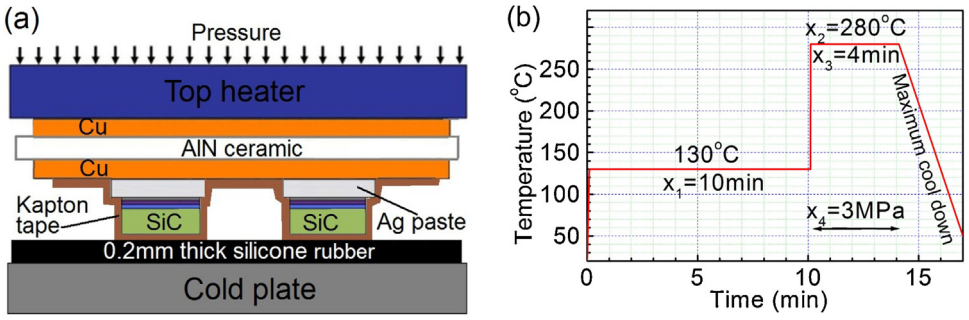

Fig. 2. Schematic diagrams of (a) sample geometry and (b) temperature and pressure profile used during the sintering process. Note that the dimensions of sample geometry are not to scale.

the bonding surface. Such a Ti\W\Au metallization was selected because, on the one hand, sputtered Ti–W can be used as the Ohmic contact metal on SiC devices and W is an effective diffusion barrier for high-temperature applications. On the other hand, it has been investigated less than Al\Ni\Ag and Al\Ni\Au metallizations commonly used in the sintering of Ag particles or nanoparticles. The bonding surfaces of the as-diced dummy SiC die all had surface roughness (Ra) < 0.001 μm.

The AlN DBC substrates were custom manufactured by Remtec, Inc (Norwood, MA 02062, USA). They consist of 1 mm thick AlN ceramic sandwiched by 0.3 mm thick Cu on both sides. The surface finish on the DBC substrates was 5 μm thick NiP followed by 0.1 μm thick Au on the top surface. The 0.1 μm thick Au layer is significantly thinner than the ~2 μm thick Ag layer plated on DBC substrates used by Wereszczak et al. (2012), and thinner than the1 μm to 4 μm thick Ag or Au layer plated on DBC substrates used by Bai and Lu (2006) and Bai et al. (2007). The bonding surfaces of the DBC substrates used in the present experiment all had surface roughness values (Ra) in the range of 1.2 μm to 2.5 μm.

2.2. Preparation of samples

Samples were bonded (SiC dies to substrate) using an in house sintering press. Fig. 1 shows the layout using 6 or 4 number, 3 mm × 3 mm × 0.35 mm dummy SiC dies on one AlN DBC substrate. For the sintering process, a layer of 100 μm thick Ag nanoparticles paste was applied on all substrates by stencil printing, followed by drying the samples at 130 °C for different times. The dummy SiC dies were then placed on the dried paste and fixed in position with Kapton tape. After this, each of the samples were then turned over and put on a piece of 0.2 mm thick silicone rubber situated on the cold plate of the sintering press. Final sintering was accomplished by rapidly applying pressure by moving down the top heater of the press (which had already reached target temperature) to contact with the top of the sample. Fig. 2 presents schematic sample geometry in situ and a representative temperature/pressure profile employed during the sintering process.

The effects of four sintering parameters were taken into account, including the time of drying the printed paste at 130 °C, the sintering temperature, pressure and time during the final sintering stage. Following Montgomery (1997), a statistical design of experiment can be used to replace the full spectrum of combined trials involving experimental parameters by the use of relatively fewer experimental trials across the scope of the experimental parameters. For example, Kingswell et al. (1993) used the Taguchi design method to optimize the vacuum plasma spray parameters for the deposition of metal, ceramic, and cermet coatings. Kim et al. (2009) employed the orthogonal design method to optimize the inter-critical annealing, ageing and galvanizing temperatures for the development of a cold rolled dual phase steel. Fang and Lin (2003) developed a relatively new statistical experiment method, the uniform design experiment. Compared with conventional statistical methods, such as the Taguchi and orthogonal design methods, this statistical experimental method decreases further the number of trials for processes involving a large number of factors. In the present work, the uniform design experiment is used, and Table 1 lists the different combinations of the four sintering parameters used and the corresponding trial codes. In Table 1, trials T1–T8 were arranged according to Table $U_8(8^3 \times 4)$ specified in the uniform design method. The design ranges of the four sintering parameters were determined from preliminary experiments to ensure that samples could be assembled with a high level of confidence. The time of drying for the printed paste at 130 °C, and the sintering pressure and time were graded

Table 1
Sintering parameters and the corresponding sample codes used to prepare the multiple die attachment samples for the shear tests.

Trial	Dring time at 130 °C, x_1, (min)	Sintering temperature, x_2, (°C)	Sintering time, x_3, (min)	Pressure x_4, (MPa)
T1	10	280	4	3
T2	15	240	8	7
T3	20	280	3	11
T4	25	240	7	15
T5	30	300	2	1
T6	35	260	6	5
T7	40	300	1	9
T8	45	260	5	13
AT1	10	240	1	1
AT2	45	300	8	15

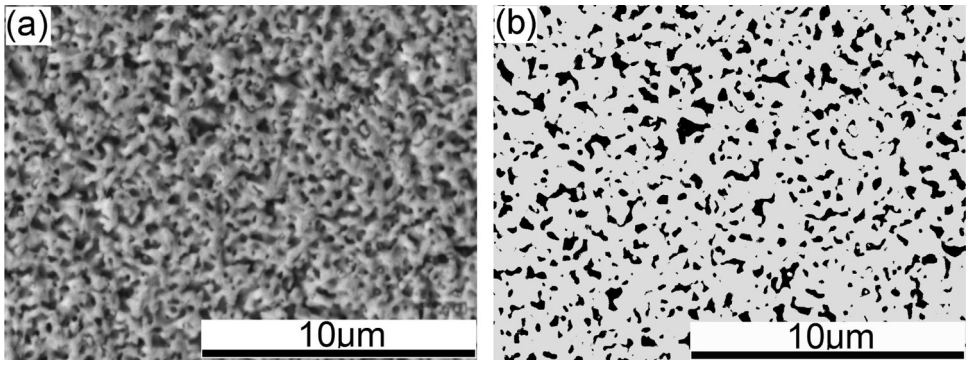

Fig. 3. (a) SEM image taken from one shear failure surface of sample T1 and (b) the corresponding black and white binary image used to calculate the apparent "porosity", i.e. 24%.

into 8 levels and the sintering temperature was graded into 4 levels. For samples T1–T8, 6 dummy SiC dies were sintered on each of the substrates as shown in Fig. 1(a). In addition, two additional trials, AT1 and AT2, were also added into the sintering experiment. They correspond to the lowest and the highest levels of the four sintering parameters used within the scope of the statistical design experiment. For both samples AT1 and AT2, only 4 dummy SiC dies have been sintered on each of the substrates as shown in Fig. 1(b).

2.3. Shear testing and characterization of samples

The shear tests were carried out on a Nordson DAGE 4000 bond-tester (Dage Holdings Limited, Aylesbury, Buckinghamshire, UK). For samples T1–T8, 5 of the 6 sintered Ag die attachments were tested, and for samples AT1 and AT2, 3 of the 4 sintered Ag die attachments were tested. For all tests, the shear forces were recorded by applying a constant shear rate of 0.3 mm/min until the SiC die was sheared off from the substrates. The shear strength values (MPa) were calculated from the recorded maximum shear forces divided by the bonding area of the die attachment, i.e. 3 mm × 3 mm (9 mm^2).

After the shear tests, the failure surfaces, i.e. the de-bonded surfaces on both the DBC substrate and the SiC die sides, were observed with a Hitachi TM3000 desktop Scanning Electronic Microscope (SEM, Hitachi High-Tech, Minato-ku, Tokyo 105-8717, Japan). As presented, the porous macrostructure of the sintered Ag die attachments can be observed from failure surfaces on the substrate sides for shear-tested samples. Therefore, a type of porosity, referred to as "apparent" porosity, was measured from the SEM images showing the porous microstructure. This was done using an image analysis method, which will now be described in reference to Fig. 3. Firstly, a threshold value for the pixel intensity was manually selected to covert the digital SEM image shown in Fig. 3(a) into a black and white binary image as shown in Fig. 3(b), ensuring that the black areas in Fig. 3(b) look representative to the pores in Fig. 3(a) in respect to size. The "apparent" porosity is then calculated by segmenting and measuring the black areas in Fig. 3(b) divided by the total area of the image.

For each sintered Ag die attachment, two images of 1280 × 960 pixels in resolution, one of 34 × 26 μm and another one of 17 × 13 μm in size, were used to measure the "apparent" porosity. The "apparent" porosity" values presented below for each sintered Ag die attachment will hence be the mean of two values measured from two SEM images. Because of the surface topology and deformation of the microstructure features after the shear test, it is felt that such an "apparent" porosity cannot represent the real porosity of each sintered Ag die attachment. However, it may still provide a relative comparison of densification among the different sintered Ag die attachments.

For most samples, the shear-induced de-bonding occurred entirely near the interfaces between the sintered Ag layer and the Ti\W\Au metallization on the SiC die. However, for a few samples, the de-bonding occurred partly at the interfaces between the sintered Ag layers and the NiP\Au finish on the DBC substrates, and partly near interfaces between the sintered Ag layer and the Ti\W\Au metallization on the SiC die. Therefore, the thicknesses of the residual Ag layers on the DBC substrates measured using a Zeta-20 3D optical profiler (Zeta Instruments, San Jose, CA 95131, USA) can be taken as approximate thickness values of the as-sintered Ag layers. For each die attachment, 5 measurements were performed and their mean was given as the resulting thickness.

3. Results

3.1. Shear strength values

The average shear strength values for the 10 multiple die attachment samples (T1–AT2) were found to be in the range of 15.7–52.5 MPa. As shown in Fig. 4, of the 10 multiple die attachment samples, 8 samples have shear strength values with moderate variations of 10–40 MPa while the other two samples, samples T7 and T8, have shear strength values with relatively wide variations of 10–100 MPa. Of the total 46 shear strength values tested there are 3 values which are lower than 10 MPa (T5 and T8) and 1 value which exceeds 110 MPa (T8)

The average shear strength values of the 10 samples have been regressed as the first and second-order polynomial equations of the four sintering parameters listed in Table 1. This was done using the

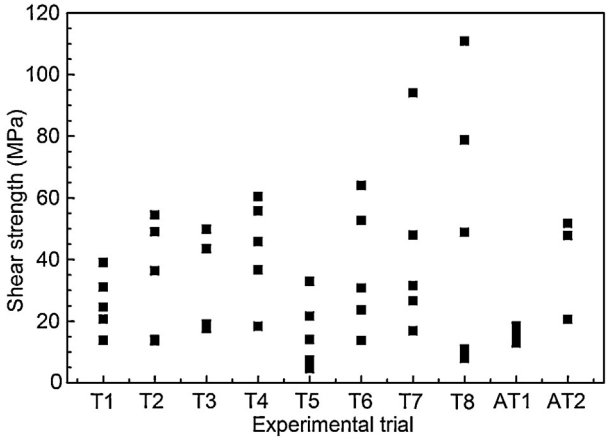

Fig. 4. The tested shear strength values of all the 46 sintered Ag die attachments on the 10 multiple die attachment samples.

Table 2
Results for the stepwise regression analysis in which the average shear strength values of the 10 multiple die attachment samples were regressed as both the first- and second-order polynomial equations of the 4 sintering parameters listed in Table 1.

Order	Equation	Source	Degrees of freedom	Mean square	Overall F	Confidence level
1	$15.24 + 2.42 \times 10^{-1}x_1 + 1.54x_4$	Regression Residual	2 7	499.5 49.95	12.31	0.99
2	$9.01 + 8.43x_4 + 7.32 \times 10^{-3}x_1{}^2 - 1.39 \times 10^{-2}x_2x_4 - 2.10 \times 10^{-1}x_4{}^2$	Regression Residual	4 5	309.1 9.34	33.11	>0.99

step regression method as described by Walpole and Myers (1978). The results are listed in Table 2 and can be used to explore the effects of the sintering parameters within the scope of the uniform design experiment on the average shear strength. According to Draper and Smith (1981), whether a regressed equation is statistically significant is judged from the confidence level, which is determined by using the F test. Following Christensen (1996), the precision of the prediction for the regressed equation is determined from the residual mean square value. For example, if the sintering parameters are x_1, x_2, x_3 and x_4, there would be probabilities approximately of 0.68 and 0.95 at which the predicted objective function, here the average shear strength, is within $F(x_1, x_2, x_3, x_4) \pm (\text{residual mean square})^{1/2}$ and $F(x_1, x_2, x_3, x_4) \pm 2(\text{residual mean square})^{1/2}$, respectively.

From Table 2, it can be seen that both the first- and second-order polynomial equations are statistically significant with confidence levels equivalent to or higher than 0.99. The regressed second-order equation has improved prediction precision of ±3.0 MPa when compared with ±7.1 MPa of the regressed first-order equation, at a probability approximately of 0.68. Both the regressed first and second-order equations reveal the effect of sintering time on the average shear strength is negligible.

Table 3 compares the experimentally tested average shear strength values of the 10 multiple die attachment samples with the values calculated from the regressed first- and the second-order equations. It can be seen that the values calculated from the regressed second-order equation are in reasonable agreement with the tested values, with a maximum absolute error of 4.3 MPa for sample T1.

Fig. 5 plots the curves of the average shear strength versus the sintering pressure for 4 different times of drying the printed paste at 130 °C and two different sintering temperatures, derived from the regressed second-order equation in Table 2. It can clearly be seen that longer drying times (of the printed paste at 130 °C) combined with a lower sintering temperature, results in a higher average shear strength. However, the effect of sintering pressure is more complicated. For a lower sintering temperature, the average shear strength increases with sintering pressure, from 1 to 11 MPa at which point it remains relatively constant as the sintering pressure increases from 11 to 15 MPa. For the higher sintering temperature, the average shear strength also increases with sintering pressure from 1 to 10 MPa but then slightly decreases with further increase in the sintering pressure from 10 to 15 MPa. Based on the regressed second-order equation within the scope of the uniform design experiment, the maximum average shear strength of 54.9 ± 3.0 MPa, can be obtained by drying the printed paste for 45 min at 130 °C, using a sintering temperature of 240 °C, and a sintering pressure of 12.5 MPa.

3.2. Damage modes of shear-tested samples

SEM observations of the failure surfaces revealed three types of damage modes for all the die attachments after the shear tests. It should be noted that the damage modes relate to the microstructural mechanisms with which de-bonding occurs during shear tests. As shown in Fig. 6, for the first observed damage mode, the majority of the sintered Ag layer remains on the DBC substrate, and exhibits a porous microstructure. There is also an indication of corrugation on the failure surface of the sintered Ag layer. In comparison, on the SiC die side, there are lots of 0.1–1 μm Ag particles covering the surface of the Ti\W\Au metallization. Therefore, it may be concluded that the de-bonding of the die attachment occurred entirely within the sintered Ag layer and very near the interfaces between the sintered Ag layer and the Ti\W\Au metallization on the SiC die. For the 46 shear-tested die attachments, two thirds of those with shear strength values lower than 45 MPa de-bonded with this damage mode.

The second observed damage mode is shown in Fig. 7. In this damage mode case, most of the de-bonding area of the die attachment occurs within the sintered Ag layer (as seen in Fig. 6) and near the interfaces between the sintered Ag layer and the Au metallization on the SiC die, as seen previously. However, a relatively small ratio of the bonding area of the die attachment also de-bonded at the interface between the sintered Ag layer and the NiP\Au metallization on the DBC substrate. This is clearly shown in Fig. 7(c) where an area of Ag sintered layer still remains on the SiC die after shear test. One third of the die attachments with shear strength values lower than 45 MPa exhibited this type of damage mode.

In comparison all die attachment samples with shear strength values higher than 45 MPa exhibited the third observed damage mode. The de-bonding occurred partly within the sintered Ag layer, near the interface between the sintered Ag layer and the Ti\W\Au metallization on the SiC die side, and partly at the interface between the sintered Ag layer and the NiP\Au metallization on the DBC substrate side, a combination of the first and second observed damage modes. Additionally, peeling of the Ti\W\Au metallization from the SiC die was also observed (area C) as shown in Fig. 8, with small areas covered with Ti\W\Au on the failure surface of the DBC side. However, in contrast to the observed second damage mode, the sintered Ag layer appears much denser. In addition, there also appears to be some broken SiC debris on the DBC substrate side, although not all the failure surfaces on the DBC substrate sides (of the die attachments exhibiting this third damage mode) showed this.

3.3. Correlation with porosity and thickness

The relationships between the shear strength and both the "apparent" porosity and the thickness of the sintered Ag attachments are presented in Figs. 9 and 10, where R in both figures stands for the coefficient of correlation for linear data fitting. It should be pointed out that the linear data fitting between the individual shear strength and the "apparent" porosity for all the 46 die attachments is actually better than that for the average shear strength and the average "apparent" porosity. Similarly, the linear data fitting of the relationship between the individual shear strength and the thickness is better than for that between the average shear strength and the average thickness, for all samples. This is because the goodness of linear data fitting is tested by both the coefficient of correlation (R) and the number of data points, as described by Draper and Smith (1981).

Comparing the linear data fitting of the relationship between the shear strength and the "apparent" porosity with the corresponding linear data fitting of the relationships between the shear

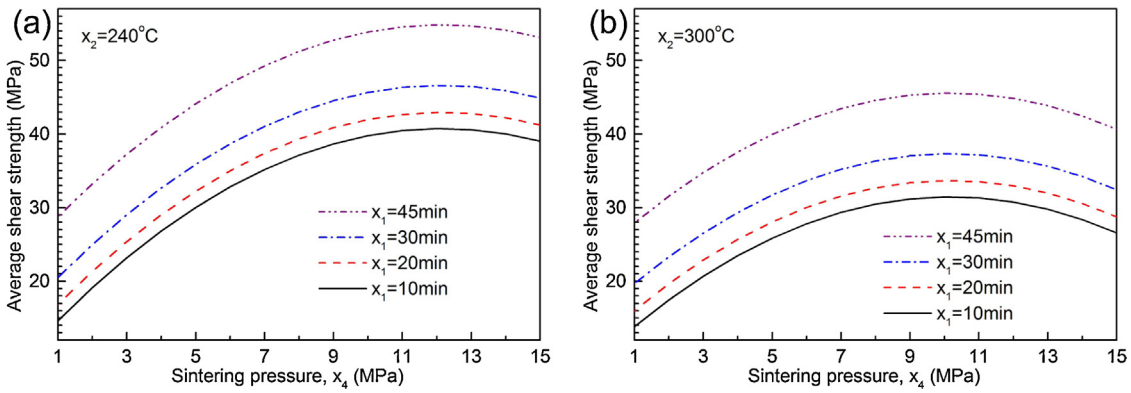

Fig. 5. Plots of average shear strength versus sintering pressure for 4 different times of drying the printed paste at 130 °C, x_1, and 2 different sintering temperatures: (a) x_2 = 240 °C and (b) x_2 = 300 °C, which are derived from the regressed second-order equation listed in Table 2, regardless of the sintering time, x_3, 1–8 min.

strength and the thickness, we find that the former linear data fitting is slightly better than the latter. Nevertheless, based on the R values and numbers of data points, all four linear data fittings in Figs. 9 and 10 are highly significant, with confidence levels of 0.99 or even higher. Therefore, it can be seen that in a statistical sense, the lower the "apparent" porosity and the thickness, the higher the shear strength of the sintered Ag die attachment.

4. Discussion

The variations in the presented shear strength values for each of the multiple die attachment samples may be attributed to variations in thickness and uniformity of the printed Ag paste and in the pressure applied on the 6 or 4 dies during the sintering process. In order to test this hypothesis, after shear tests, the flatness of the 10 DBC substrates was measured, and surface flatness was found to be in the range of 6–15 μm. It is therefore concluded that surface warpage has resulted in both a non-uniform thickness of the printed Ag paste, and non-uniform pressure being applied on the different dies during the sintering process; even though a 0.2 mm thick flexible silicone rubber was situated on the cold plate of the sintering press (under the sample) as shown in Fig. 2(a) for compliance.

Despite the variation in the tested shear strength values for each of the samples, the average shear strength values and their variations are comparable with those reported in the existing literature. For example, Bai and Lu (2006) attached 1.706 mm × 1.380 mm SiC devices with 1.4 μm thick Ni\Ag metallization on a DBC substrates coated with 4 μm thick Ag or Au using pressure-less sintering of Ag nanoparticles at 300 °C for 10–90 min. The average shear strength

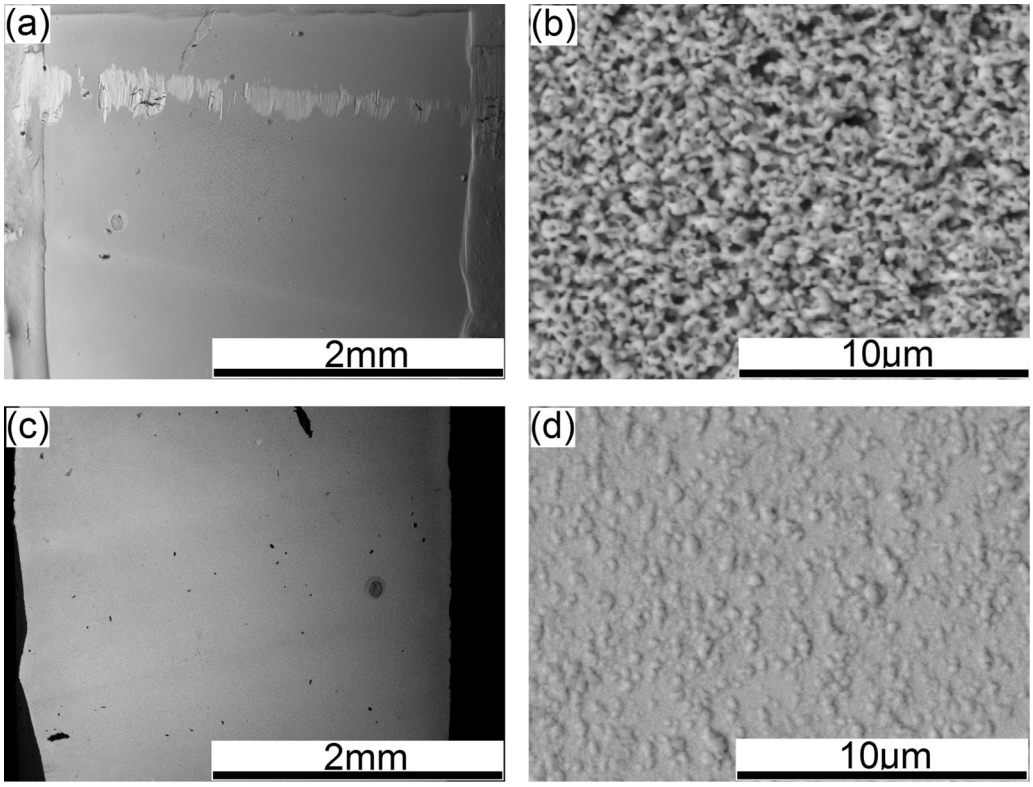

Fig. 6. SEM images taken from the failure surfaces of one die attachment of sample T1 with shear strength of 13 MPa: (a) overview of the failure surface on the DBC side; (b) enlarged view showing porous sintered Ag layer on the DBC side; (c) overview of the failure surface on the SiC die side; (d) enlarged view showing 0.1–1 μm Ag particles partly covering the surface of the Ti\W\Au metallization on the SiC die.

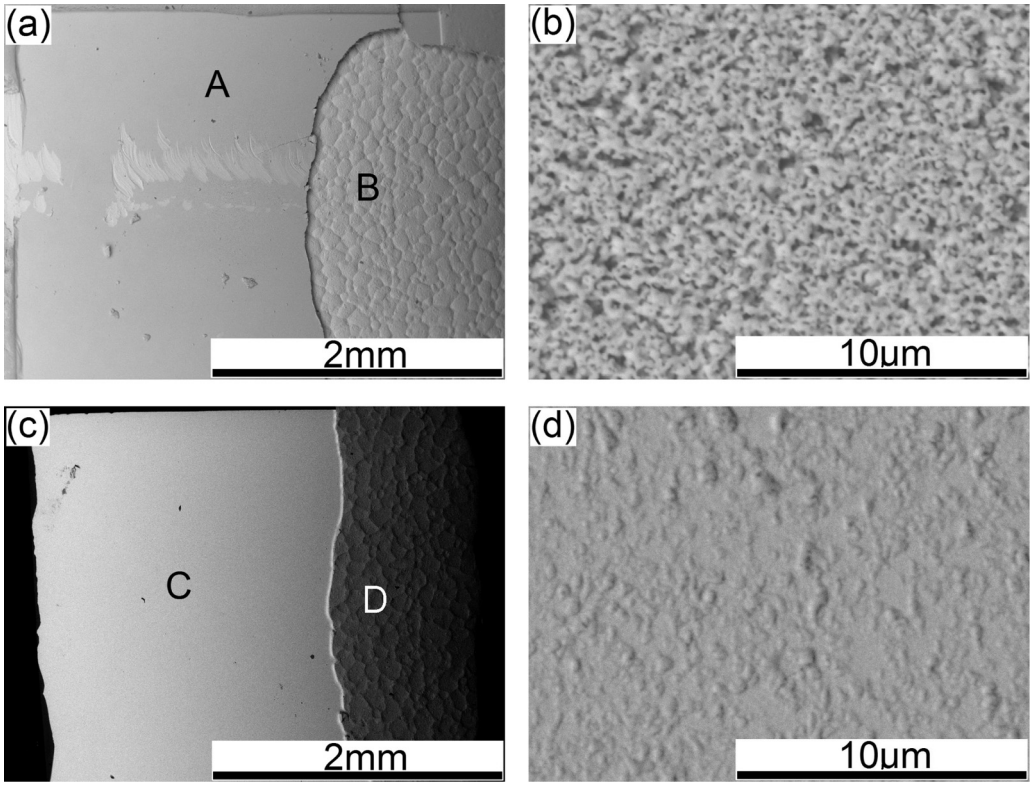

Fig. 7. SEM images taken from the failure surfaces of one die attachment of sample AT1 with shear strength of 18 MPa: (a) overview of the failure surface on the DBC side; (b) enlarged view of showing porous sintered Ag layer at location A of image (a); (c) overview of the failure surface on the SiC die side; (d) enlarged view showing 0.1–1 μm Ag particles partly covering the surface of the Ti\W\Au metallization at location C of image (c). B in image (a) points at the area where the de-bonding occurred at the interface between the sintered Ag layer and the NiP\Au metallization on the DBC substrate; and D in image (c) points at the area where the sintered Ag layer remained on the SiC die side.

values of the die attachments on the Ag-coated DBC substrates were in the range of 15–43 MPa, while those of the die attachments on the Au-coated DBC substrates in the range 5–25 MPa. The latter values (5–25 MPa) are similar to the present tested average shear strength values of the die attachments produced under pressures of 1–2 MPa. Buttay et al. (2011) prepared single die attachment samples of 2.7 mm × 2.7 mm dummy SiC dices with Ag metallization on DBC substrates using pressure-assisted sintering of Ag nanoparticles at 285 °C and 6 MPa for 60 min, with consideration of Cu surface finish, Au finish and surface roughness of the DBC substrates. For each consideration of the DBC substrates, 6 samples were repeated. The reported average shear strength values were ~7–31 MPa and the variations in the shear strength values, for most substrates, were in the range of 20–45 MPa. Such variations in the shear strength values are similar to the variations for the present multiple die attachment samples. Wereszczak et al. (2012) prepared samples of single DBC substrates joined on similar DBC substrates plated with ~2 μm thick Ag using pressure-assisted sintering of micron-sized Ag particles at 280 °C and 30 MPa for 10 min, with consideration of substrate topography and attachment pad geometry. The joining area was 8 mm × 8 mm, and 3 or 4 samples were repeated for each consideration. The average shear strength values were 10.7–51.7 MPa for the different considerations and the variations in the shear strength values for most considerations

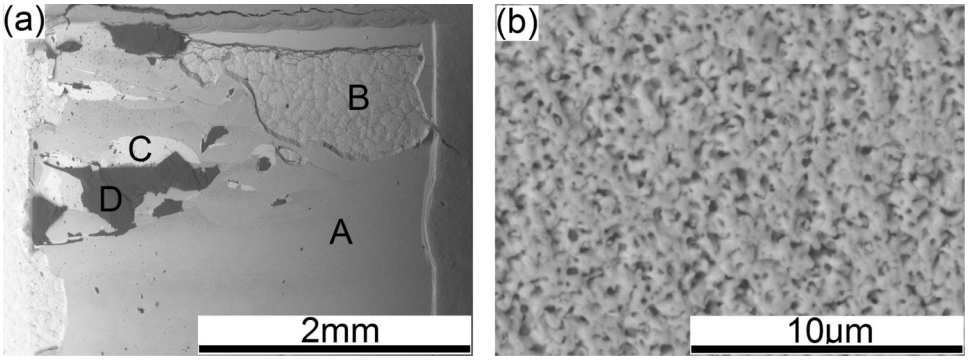

Fig. 8. SEM images taken from the failure surface on the DBC side of one die attachment of sample T8 with shear strength of 78 MPa: (a) overview of the failure surface showing three distinctive areas A, B, C, (b) enlarged view of showing relatively dense sintered Ag layer at location A of image (a). In image (a), A points at the area where the sintered Ag layer remained on the DBC substrate; B points at the area where the de-bonding occurred at the interface between the sintered Ag layer and the NiP\Au metallization on the DBC substrate; C points at a small area covered with the Ti\W\Au metallization peeled off from the SiC die; and D points at a small piece of broken SiC debris on the failure surface.

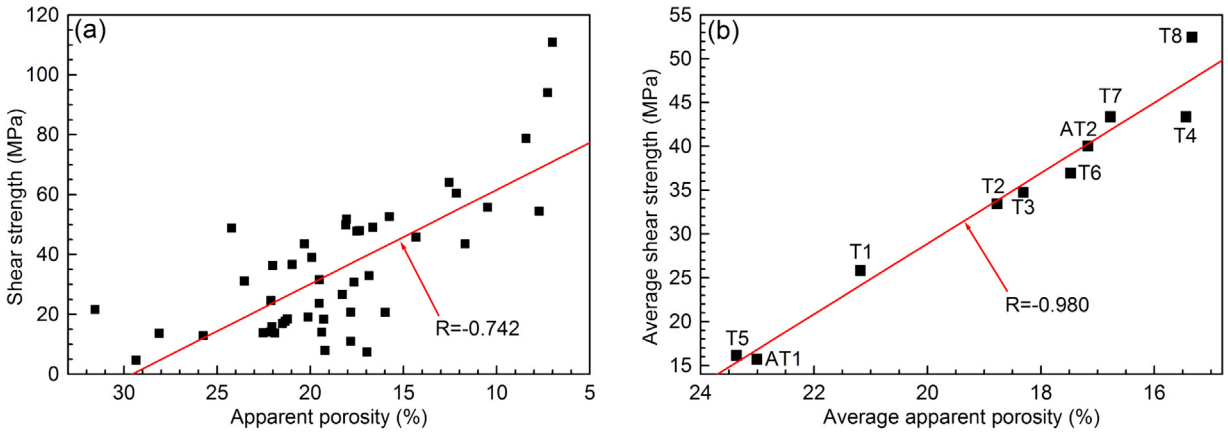

Fig. 9. Relationship between shear strength and "apparent" porosity: (a) plot of shear strength versus "apparent" porosity for all the 46 die attachments; (b) plot of average shear strength versus average "apparent" porosity for the 10 multiple die attachment samples.

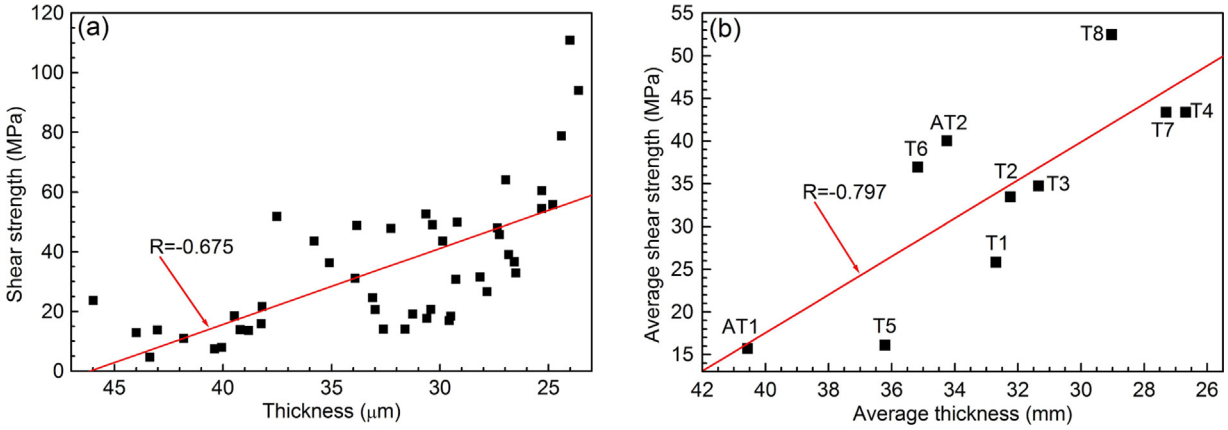

Fig. 10. Relationship between shear strength and thickness: (a) plot of shear strength versus thickness for all the 46 die attachments; (b) plot of average shear strength versus average thickness for the 10 multiple die attachment samples.

were 20–40 MPa, comparable with most of the results presented in Table 3 and Fig. 4.

The regressed equations listed in Table 2 are only valid for the average shear strength of the present multiple SiC die attachment and the sintering parameters used within the scope of the design experiment. According to the regressed second-order equation, the average shear strength increases with increased drying time for the printed paste at 130 °C. This can be ascribed to effective burnout of the organic dispersant, binder and thinner in the paste and better re-arrangement of the Ag nanoparticles during the extended drying stage. The decrease in average shear strength with increasing sintering temperature may be related to rapid growth and coalescence of the Ag nanoparticles at higher sintering temperatures. This is because with too rapid a growth and coalescence of Ag nanoparticles, it is more difficult for the particles to further re-arrange during the final sintering stage, which would lead to relatively non-uniform and large particles and pores within the sintered Ag layer. This can be verified by the SEM images shown in Figs. 6(b) and 7(b), which were taken from die attachments prepared at 280 °C and 240 °C, respectively. As aforementioned, the de-bonding for most die attachments occurred within the sintered Ag layer, near the interface between the sintered Ag layer and the Au metallization on the SiC die. Therefore, it is probably true to say that the relatively non-uniform and large particles and pores within the sintered Ag layer result in decreasing average shear strength as the sintering temperature increases.

Table 3
Comparison of the tested average shear strength values with the values calculated from the regressed equations listed in Table 2.

Trial	Tested value (MPa)	Value from the first-order equation (MPa)	Relative error (%)	Value from the second-order equation (MPa)	Relative error (%)
T1	25.8	22.3	−13.8	21.5	−16.8
T2	33.5	29.6	−11.4	36.1	7.9
T3	34.7	37.0	6.5	36.6	5.2
T4	43.4	44.4	2.3	42.9	−1.1
T5	16.1	24.0	49.2	19.7	22.0
T6	36.9	31.4	−15.0	36.9	−0.2
T7	43.4	38.8	−10.6	42.2	−2.8
T8	52.5	46.1	−12.1	51.1	−2.7
AT1	15.7	19.2	22.2	14.6	−6.8
AT2	40.1	49.2	22.9	40.6	1.5

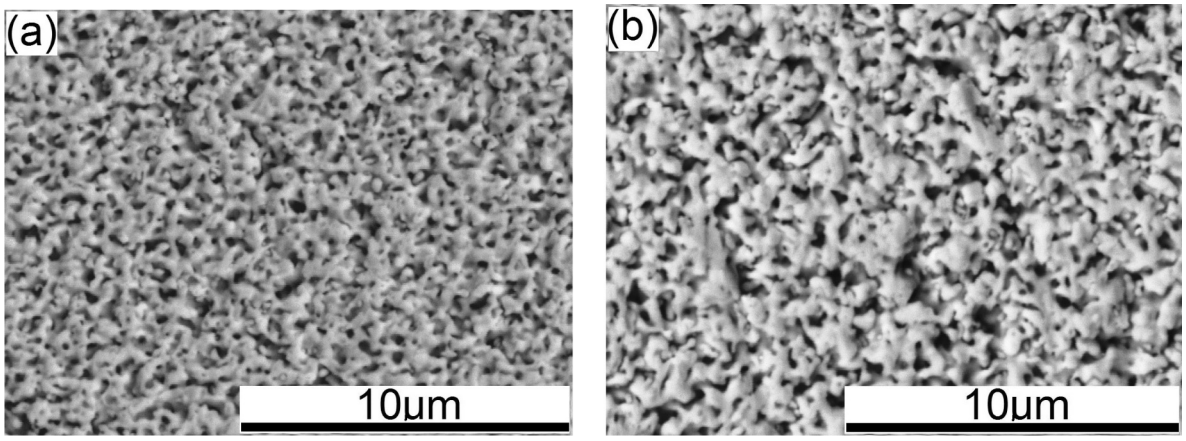

Fig. 11. SEM images taken from the failure surfaces of one die attachment of: (a) sample T7 with shear strength of 47 MPa and "apparent" porosity of 17.4%; (b) sample AT2 with shear strength of 51 MPa and "apparent" porosity of 18.0%.

At low sintering temperatures, the present effect of the sintering pressure on the average shear strength as shown in Fig. 5(a) is similar to that reported by Zheng et al. (2012) on the average shear strength of low-pressure sintered Ag joints. The increase in the average shear strength with increasing sintering pressure may be explained in terms of atomic diffusion and particle consolidation enhanced by the sintering pressure. However, at higher sintering temperatures, the present average shear strength appears to slightly decrease with further increases in sintering pressure from 10 to 15 MPa. This is hard to understand and explain, but may also be related to rapid growth and coalescence of Ag nanoparticles at both higher sintering temperature and higher sintering pressures. The latter statement can be partly supported by the two SEM images shown in Fig. 11, taken from the failure surfaces of two die attachments both processed at 300 °C. Due to rapid growth and coalescence of the Ag nanoparticles, the pores/voids in die attachment AT2 formed under 15 MPa are clearly larger and more irregular than those in die attachment T7 formed under 9 MPa.

Unlike the results reported by Bai and Lu (2006), where the average shear strength of the die attachments produced using pressure-less sintering of Ag nanoparticles increased with sintering time (from 10 to 90 min), the effect of sintering time on the average shear strength in the present work is negligible. This difference may be attributed to the following two facts; the sintering times used in the present work are relatively short, in the range 1–8 min, and the present SiC die were placed on printed paste which had already been dried at 130 °C. Re-arrangement of the Ag nanoparticles and subsequent atomic diffusion and particle consolidation during the final sintering stage may already be completed within 1 or 2 min, and as a result, increasing the sintering time beyond this will have no or little effect on the average shear strength in the present work.

The observed shear-induced damage modes in the present work are also different from those reported previously. This difference may also be associated with the placement of the SiC dies on the dried paste of the Ag nanoparticles when compared with those where Bai and Lu (2006) placed the SiC dies on the printed wet paste of the Ag nanoparticles in their work, or alternatively, with the relatively low pressures when compared with those applied by Wereszczak et al. (2012) in their work. Because of the placement of the SiC die on the dried paste, the wetting and spreading of Ag on the surface of the Ti\W\Au metallization on the SiC die can only be achieved through solid-state atomic diffusion during the final sintering stage. Consequently, the bonding of the sintered Ag layer to the Ti\W\Au metallization would be the weakest location unless sufficiently high pressure was applied. This may explain why the present de-bonding for most die attachments with lower shear strength values occurred near the surface of the Ti\W\Au metallization on the SiC die. With relatively high pressure, on the SiC die, the solid-state atomic diffusion of the Ag into the Ti\W\Au metallization was effectively improved. In this case, the bonding strength between the sintered Ag layer and the Ti\W\Au metallization might become normalized to the bonding strength between the sintered Ag layer and the DBC substrate. This is probably the reason why the de-bonding for those die attachments with higher shear strength values occurred partly near the surface of the Ti\W\Au metallization on the SiC die and partly near the surface of the NiP\Au metallization on the DBC substrate.

The significant linear relationships between the shear strength and both the "apparent" porosity and thickness for all the 46 die attachments reveal that the distribution of the sintering pressure on the 6 or 4 SiC dies on each of the 10 multiple die attachment samples were indeed non-uniform. This is because the die attachments with higher shear strength, lower "apparent" porosity and thinner thickness values were obviously subjected to high local pressures during the sintering process than for those with lower shear strength, higher "apparent" porosity and thicker thickness values. The final thicknesses of the sintered Ag die attachments are therefore more readily influenced, as expected, by the variation in the thicknesses of the printed pastes of the Ag nanoparticles on the DBC substrates. This may be the reason why the linear relationship between the shear strength and thickness is slightly worse than that between the shear strength and the "apparent" porosity.

However, the linear relationships between the shear strength and the thickness should be more useful than the linear relationship between the shear strength and the "apparent" porosity in respect to evaluation. This is because thicknesses of the sintered Ag die attachments can be easily and conveniently tested with a non-destructive technique, e.g. an optical profiler. Given the fact that the majority of the pores/voids in the sintered Ag die attachments were smaller than one micron (Fig. 3(b)), it is very difficult, if not impossible, to detect them with non-destructive imaging technique. Therefore, the thicknesses of sintered Ag die attachments may be considered as a valid measurement to monitor the quality of die attachment during the manufacturing/assembly process. It should be the noted, however, that the linear relationship between the shear strength and the thickness has been established on a statistical basis. It may be used to identify those sintered Ag die attachments which have a probability of having a weak bonding strength, although individual samples with thinner thickness may still have lower bonding strengths than those with thicker thicknesses.

Based on the regressed second-order equation listed in Table 2, the maximum average shear strength that can be achieved from the present multiple die attachment samples are 54.9 ± 3.0 MPa. However, the maximum individual shear strength that has been obtained is 110 MPa (Fig. 4). Therefore, an average shear strength higher than the present maximum 54.9 ± 3.0 MPa should be achievable if the uniformity of the thickness of the printed Ag paste, the flatness of the DBC substrate and the pressure applied on the die are all improved. This should be more easily accomplished on single die attachment samples with increased sintering pressure. In addition, as aforementioned, the Au finishes on the present dummy SiC dice and the DBC substrates are very thin compared with those of ~2 μm thick Ag finish which Wereszczak et al. (2012) used and 1 μm to 4 μm thick Ag or Au finishes which Bai and Lu (2006) used. Therefore, further work is also needed to investigate and demonstrate the effect of the thicknesses of the metallization finishes on both the die and DBC substrates on resultant bond strength.

5. Conclusions

- The maximum individual shear strength value obtained is 110 MPa, and the variations in the average shear strength values for most multiple die attachment samples are 10–40 MPa. The variations can be attributed to non-uniform thickness of the printed Ag pastes and pressure applied on the dies.
- The average shear strength of the multiple die attachment samples depends on the Ag paste drying time, sintering temperature and pressure in a nonlinear manner. This can be explained with the effectiveness of the organic content burnout and appropriate rate of growth and coalescence of the Ag nanoparticles.
- The de-bonding for most die attachments with lower shear strength occurred near the surface of the Ti\W\Au metallization on the SiC die, while for those die attachments with higher shear strength occurred partly near the surface of the Ti\W\Au metallization on the SiC dies and partly near the surface of the NiP\Au metallization on the DBC substrate.
- Significant linear relationships exist between the shear strength and both the “apparent” porosity and thickness for all die attachments. The measured thicknesses of sintered Ag die attachments may be used as a good indicator to monitor the quality of die attachments during the manufacturing/assembly process.

Acknowledgements

This research was supported by the UK Engineering and Physical Science Research Council as part of the Innovative Electronic Manufacturing Research Centre (IeMRC) [grant number EP/H03014X/1] and the European Union’s Clean Sky JTI - Systems for Green Operations ITD. The authors wish to thank Oscar Khaselev and Mike Marczi of Cookson Electronics for providing the paste of Ag nanoaprticles.

References

Akada, Y., Tatsumi, H., Yamaguchi, T., Hirose, A., Morita, T., Ide, E., 2008. Interfacial bonding mechanism using silver metallo-organic nanoparticles to bulk metals and observation of sintering behaviour. Mater. Trans. 49 (7), 1537–1545.

Amagai, M., 2008. A study of nanoparticles in Sn–Ag based lead free solders. Microelectron. Reliab. 48 (1), 1–16.

Bai, J.G., Lu, G.Q., 2006. Thermomechanical reliability of low-temperature sintered silver die attached SiC power device assembly. IEEE Trans. Device Mater. Reliab. 6 (3), 436–441.

Bai, J.G., Yin, J., Zhang, Z., Lu, G.Q., van Wyk, J.D., 2007. High-temperature operation of SiC power devices by low-temperature sintered silver die-attachment. IEEE Trans. Adv. Packag. 30 (3), 506–510.

Buttay, C., Masson, A., Li, J., Johnson, M., Lazar, M., Raynaud, C., Morel, H., 2011. Die attach of power devices using silver sintering – bonding process optimisation and characterization. In: Proceedings of The International Conference and Exhibition on High Temperature Electronics Network (HiTEN 2011), July 18–20, 2011, Oxford, UK, pp. 84–90.

Christensen, R., 1996. Analysis of Variance, Design and Regression. Chapman & Hall, London, UK.

Draper, N.R., Smith, H., 1981. Applied Regression Analysis. Wiley, New York.

Fang, K.T., Lin, D.K.J., 2003. Uniform experimental design and their applications in industry. In: Khattree, R., Rao, C.R. (Eds.), Handbook of Statistics, vol. 22. Elsevier Science B.V., pp. 131–170.

Hamada, K., 2012. SiC device and power module technologies for environmentally friendly vehicles. In: Proceedings of 7th International Conference on Integrated Power Electronics Systems, March 6–8, 2012, Nuremberg, Germany, pp. 473–477.

Ide, E., Angata, S., Hirose, A., Kobayashi, K.F., 2005. Metal-metal bonding process using Ag metallo-organic nanoparticles. Acta Mater. 53 (8), 2385–2393.

Kaminski, N., 2012. SiC and GAN devices – competition or coexistence? In: Proceedings of 7th International Conference on Integrated Power Electronics Systems, March 6–8, 2012, Nuremberg, Germany, pp. 393–403.

Kim, S.J., Cho, Y.G., Oh, C.S., Kim, D.E., Moon, M.B., Han, H.N., 2009. Development of a dual phase steel using orthogonal design method. Mater. Design 30, 1251–1257.

Kingswell, R., Scott, K.T., Wassell, L.L., 1993. Optimizing the vacuum plasma spray deposition of metal, ceramic, and cermet coatings using designed experiments. J. Therm. Spray Technol. 2, 179–186.

Kraft, S., Schletz, A., Marz, M., 2012. Reliability of silver sintering on DBC and DBA substrates for power electronic applications. In: Proceedings of 7th International Conference on Integrated Power Electronics Systems, March 6–8, 2012, Nuremberg, Germany, pp. 439–444.

Laurila, T., Vuorinen, V., Kivilahti, J.K., 2005. Interfacial reactions between lead-free solders and common base materials. Mater. Sci. Eng. Rep. 49 (1-2), 1–60.

Le Henaff, F., Azzopardi, S., Woirgard, E., Deletage, J.-Y., Bontemps, S., Joguet, J., 2012. A preliminary study on the thermal and mechanical performances of sintered nano-scale silver die-attach technology depending on the substrate metallization. Microelectron. Reliab. 52 (9-10), 2321–2325.

Li, J.F., Agyakwa, P.A., Johnson, C.M., 2012. Effect of trace Al on growth rates of intermetallic compound layers between Sn-based solders and Cu substrate. J. Alloys Compd. 545, 70–79.

Li, J.F., Mannan, S.H., Clode, M.P., Johnston, C., Crossley, A., 2007. Dissolution and interfacial reaction of Nb in contact with the molten 52In–48Sn solder. Acta Mater. 55 (15), 5057–5071.

Li, X., Chen, G., Chen, X., Lu, G.Q., Wang, L., Mei, Y.H., 2013. High temperature ratcheting behavior of nano-silver paste sintered lap shear joint under cyclic shear force. Microelectron. Reliab. 53 (1), 174–181.

Lugscheider, E.F., Ferrara, S., 2004. Characterisation and optimization of innovative solders for transient liquid phase bonding and active soldering. Adv. Eng. Mater. 6 (3), 160–163.

Mannan, S.H., Clode, M.P., 2004. Materials and processes for implementing high-temperature liquid interconnects. IEEE Trans. Adv. Packag. 27 (3), 508–514.

Schwarzbauer, H., 1987. Method for mounting electronic components on a substrate. EPO Patent EP0242626.

Montgomery, D.C., 1997. Design and Analysis of Experiments. John Wiley & Sons, New York, USA.

Takaku, Y., Makino, K., Watanabe, K., Ohnuma, I., Kainuma, R., Yamada, Y., Yagi, Y., Nakagawa, I., Atsumi, T., Ishida, K., 2009. Interfacial reaction between Zn–Al-based high-temperature solders and Ni substrate. J. Electron. Mater. 38 (1), 54–60.

Walpole, R.E., Myers, R.H., 1978. Probability and Statistics for Engineers and Scientists, second ed. Macmillan, New York.

Wang, J., Besnoin, E., Duckham, A., Spey, S.J., Reiss, M.E., Knio, O.M., Powers, M., Whitener, M., Weihs, T.P., 2003. Room-temperature soldering with nanostructured foils. Appl. Phys. Lett. 83 (19), 3987–3989.

Wereszczak, A.A., Vuono, D.J., Liang, Z., 2012. Sintered silver joint strength dependence on substrate topography and attachment pad geometry. In: Proceedings of 7th International Conference on Integrated Power Electronics Systems, March 6–8, 2012, Nuremberg, Germany, pp. 451–456.

Zheng, H., Calata, J., Ngo, K., Luo, S., Lu, G.Q., 2012. Low-pressure (<5 MPa) low-temperature joining of large-area chips on copper using nanosilver paste. In: Proceedings of 7th International Conference on Integrated Power Electronics Systems, March 6–8, 2012, Nuremberg, Germany, pp. 445–450.

Zhang, Z., Lu, G.Q., 2002. Pressure-assisted low-temperature sintering of silver paste as an alternative die-attach solution to solder reflow. IEEE Trans. Electron. Packag. Manuf. 25 (4), 279–283.